Available online at www.sciencedirect.com
ScienceDirect
Journal of Computational Physics 217 (2006) 642–657
JOURNAL OF COMPUTATIONAL PHYSICS
www.elsevier.com/locate/jcp

Finite difference approximations of first derivatives for two-dimensional grid singularities

Herwig A. Grogger *

University of Applied Sciences FH Joanneum, Automotive Engineering, Alte Poststrasse 149, A-8010 Graz, Austria

Received 13 April 2005; received in revised form 11 January 2006; accepted 12 January 2006
Available online 21 February 2006

Abstract

Explicit finite difference approximations of first derivatives are developed for two-dimensional three-way and five-way grid singularities. The schemes for three-way singularities also apply for six-way singularities. The development objectives are such that the finite difference schemes are non-dissipative and compatible with regular difference approximations for convection dominated phenomena. Special emphasis is given to the directional dependency of numerical phase speeds and stability limits for explicit time integration. For that purpose, free coefficients are used to minimize the isotropy error of the numerical phase velocity. It is shown that numerical phase speeds and stability limits are almost isotropic. Hence, employment of the proposed schemes is nearly independent of the local orientation of the differencing stencil. The time step limits are greater than those of regular finite differences, indicating that the overall time step of a computation is not reduced by employing the proposed schemes. The developed schemes for three-way singularities are of second, fourth and sixth order of accuracy, whereas the five-way difference approximations are second and fourth order accurate, respectively.

The spectral characteristics, the formal order of accuracy and the stability limits of the proposed schemes imply that they can favorably be used in combination with regular difference approximations of the same order of accuracy on block-structured grids.

Keywords: Finite difference; Grid singularity; Linear wave-propagation; Isotropy error; Numerical stability

1. Introduction

Finite differences are a classical means to discretize spatial derivatives of partial differential equations. They can be formulated to achieve very high accuracy and very good spectral characteristics [1,2], but it is well known that they lack some flexibility in treating complex grid arrangements. For points, which do not exhibit regular differencing stencils, accuracy of the solution of hyperbolic problems may become poor [3]. Several methods have been developed, which allow to treat unstructured grids. In the context of convection dominated

* Tel.: +43 316 5453 8457; fax: +43 316 5453 8401.
E-mail address: herwig.grogger@fh-joanneum.at.

0021-9991/$ - see front matter
doi:10.1016/j.jcp.2006.01.017

phenomena, formulations based on finite volumes, discontinuous Galerkin method and mesh-less methods are representatives of modern developments.

Nevertheless, finite differences are attractive. They can be evaluated very efficiently by computers, if structured i,j,k-addressing is possible [4]. The purpose of the current work is to develop finite difference approximations of first derivatives for points of two-dimensional grids, which do not exhibit a regular i,j,k-differencing stencil. These finite differences are intended to be used in grid singularities, which can arise, if blocks of regular i,j,k-addressed meshes are connected.

Chung [5] proposed "generalized finite differences", which use an irregular stencil of grid points just adequate to solve for the derivatives in the truncated Taylor series expansion. That is, the number of involved grid points is according to the required order of accuracy. The approach for mesh-less methods is similar with regard of using truncated Taylor series expansions. The approach in the current work is vice versa: the differencing stencils are determined by a given grid arrangement and comprise a certain number of points, which are used to solve for the coefficients. Consequently, the number of constraints to determine the coefficients by matching the truncated Taylor series expansions is less than the number of points involved. As a result, there are undetermined coefficients. These undetermined coefficients are found such that the emerging finite difference schemes have desired characteristics: firstly, the isotropy error of the phase speed is minimized, so that the phase speed is nearly independent of the local orientation of the differencing stencil with respect to the global coordinate system; secondly, the difference schemes are designed to be non-dissipative, which guarantees numerical stability in all directions of propagation.

Finite differences on non-rectangular grids have been developed for decades. Collatz [6] gives difference approximations on regular triangular grids for the Laplace-operator (∇^2) and the ∇^4-operator. Zingg and Lomax [7] studied several finite difference approximations for hyperbolic equations on regular triangular meshes in terms of anisotropy of the phase velocity. Mullen and Belytschko [8] investigated discretizations of the two-dimensional wave-equation on several meshes and with different discretization schemes, among others finite difference formulations. Studies on the spectral characteristics and discretization errors of two-dimensional finite difference approximations of hyperbolic equations have been presented, for example, by Vichnevetsky and Bowles [9], Vichnevetsky [10], Trefethen [11] and Bamberger et al. [12].

Optimization of finite difference schemes have been performed with different objectives. Vichnevetsky and De Schutter [13] proposed an empirically optimized scheme to improve the spectral error of discretizations of the one-dimensional convection equation. Tam and Webb [14] optimized a one-dimensional finite difference scheme with respect to minimum dispersion error in a certain wave-number range. They reduced the formal order of accuracy of the scheme to set one coefficient free, which is found by minimizing the dispersion error. Haras and Ta'asan [15] constructed compact finite difference schemes and minimized the global error taking into account the influence of time integration. Optimized finite differences were compared to conventional schemes in terms of accuracy in the context of wave-propagation phenomena by Lockard [16].

The current paper is organized as follows: Section 2 reviews Fourier analysis of discretizations of hyperbolic equations. Section 3 discusses requirements on differencing schemes for non-rectangular grids for convection dominated phenomena. In Sections 4 and 5 schemes for three-way and five-way singularities are presented, respectively. In Section 6 stability of the proposed schemes is investigated with respect to explicit time integration. Section 7 discusses results, numerical examples are given in Section 8, and a summary and conclusion closes the paper.

2. Fourier analysis of discretizations for linear wave propagation

This section presents a short overview of Fourier analysis of discretizations of two-dimensional wave-propagation, and is included to clarify terminology. A comprehensive description of Fourier analysis of discretization errors of hyperbolic equations can be found in [9].

To analyse discretizations of convection dominated phenomena, the two-dimensional linear convection equation is considered,

$$U = U(x,y,t): \quad \frac{\partial U}{\partial t} + c\cos\alpha\frac{\partial U}{\partial x} + c\sin\alpha\frac{\partial U}{\partial y} = 0, \quad c > 0, \tag{1}$$

with c denoting the absolute velocity of wave propagation, and α is the angle of propagation with respect to the x-axis. Approximating both spatial derivatives at position i by finite differences involving N neighbouring points,

$$\left.\frac{\partial U}{\partial x}\right|_i \approx \frac{1}{L}\sum_{j=0}^{N} a_{x,j}u_{i+j}, \quad \text{and} \quad \left.\frac{\partial U}{\partial y}\right|_i \approx \frac{1}{L}\sum_{j=0}^{N} a_{y,j}u_{i+j}, \tag{2}$$

with u_i denoting the approximation of U at position i, and L being the point-to-point distance, gives the semi-discretized version of (1),

$$\frac{\mathrm{d}u_i}{\mathrm{d}t} = -c\cos\alpha\frac{1}{L}\sum_{j=0}^{N} a_{x,j}u_{i+j} - c\sin\alpha\frac{1}{L}\sum_{j=0}^{N} a_{y,j}u_{i+j}, \tag{3}$$

for the discrete variable u_i. Space Fourier transformation allows to evaluate the spectral characteristics of the spatial approximation,

$$\frac{\mathrm{d}\hat{u}}{\mathrm{d}t} = H(k,\alpha)\hat{u}, \tag{4}$$

with $\hat{u}$ denoting the discrete Fourier transform of u_i, $H(k,\alpha)$ is the spectral function of the spatial approximation, and k stands for the wave-number, i.e. the spatial frequency. The real part of $H(k,\alpha)$ is connected with the dissipative characteristics of the discretization, whereas the imaginary part can be related to the propagation velocity of waves. Comparing (4) with the corresponding analytic expression

$$\frac{\mathrm{d}\hat{U}}{\mathrm{d}t} = -\mathrm{i}ck\hat{U}, \quad \mathrm{i} = \sqrt{-1}, \tag{5}$$

yields the correlation between the numerical phase speed and the true phase speed of waves. The numerical phase speed is

$$c^* = -\frac{\mathrm{Im}[H(k,\alpha)]}{k}. \tag{6}$$

Obviously, c^* is a function of the wave-number and the propagation angle. Since the true phase speed is constant, any deviation of c^* is erroneous. The ratio of numerical phase speed to true phase speed can be rewritten,

$$\frac{c^*}{c} = \frac{1}{kL}\left[\cos\alpha\sum_{j=0}^{N} a_{x,j}\sin(\vec{k}\cdot\vec{x}_j) + \sin\alpha\sum_{j=0}^{N} a_{y,j}\sin(\vec{k}\cdot\vec{x}_j)\right], \tag{7}$$

where $\vec{k}$ denotes the wave-number vector $\vec{k} = k(\cos\alpha;\sin\alpha)^{\mathrm{T}}$, and $\vec{x}_j$ is the vector of relative position of the point j with respect to point i.

For a spatial discretization to be non-dissipative, the real part of the spectral-function has to vanish,

$$\mathrm{Re}[H(k,\alpha)] = -\frac{c}{L}\left[\cos\alpha\sum_{j=0}^{N} a_{x,j}\cos(\vec{k}\cdot\vec{x}_j) + \sin\alpha\sum_{j=0}^{N} a_{y,j}\cos(\vec{k}\cdot\vec{x}_j)\right] = 0. \tag{8}$$

For any propagation angle α this can only be fulfilled, if the point arrangement of the differencing stencil is symmetric, and the coefficients a_x and a_y corresponding to a pair of symmetric points are antisymmetric. It has to be noted that up to this point no restriction has been made on the grid. For a non-dissipative approximation, the only restriction on the point arrangement is a symmetric stencil.

3. Requirements on differencing schemes for grid singularities

In two spatial dimensions, regular – or structured – grids are characterized by four grid-lines passing through every discrete interior point P of the calculation domain, for which a numerical solution of the considered problem is sought. This not only applies for points in the interior of an i,j-addressed block but also for

block interfaces, except for points at boundaries of the calculation domain. The values of the depending variable at the discrete neighbouring points located on the grid-lines through P may be employed to evaluate approximations of derivatives in P. Consequently, a differencing stencil in the interior of a regular grid exhibits four branches.

A two-dimensional grid singularity exists, if the number of branches N of an interior grid point is unequal to four. Grid singularities can occur, if regions of regular grids are connected to form a calculation mesh. For the point in the topological singularity, numerical differencing by regular finite difference schemes fails, since $N \neq 4$.

In two dimensions, grid singularities can be categorized by the number of blocks, which join at the singularity: the number of blocks is equal to the number of grid-lines in the singularity. Fig. 1 illustrates a three-way singularity and a five-way singularity in two-dimensions, respectively. In the current work three-, five-, and six-way singularities are treated. Though the number of joining blocks in the singularity is not limited, higher singularities are of minor practical interest in two spatial dimensions. The schemes for grid singularities are intended to be used for those few points of a calculation domain which do not exhibit a regular stencil. These few points should not reduce the time increment of any time marching procedure. Furthermore, the quality of the result should not be influenced by the singular points, i.e. the schemes for singular points should exhibit similar spectral characteristics as the schemes of the regular part of the grid, or preferably better ones. Hence, several issues have to be addressed in the context of differencing schemes for geometric singularities:

(1) *Non-dissipative approximation*
From physical point of view, the approximation of a first derivative should exhibit the same spectral characteristics, i.e. it should be non-dissipative and non-dispersive. Dispersion errors can hardly be avoided. A second reason for requiring dissipation-less schemes is numerical stability in all directions of propagation. If the scheme is dissipative, its spectral function could – depending on the angle of propagation – exceed the stability region of the time integration scheme in the complex $H(k,\alpha)$-plane, denoting a numerically unstable situation [9]. Hence, a non-dissipative approximation is a necessary condition for numerical stability to be independent of propagation direction.

(2) *Isotropy error of numerical phase velocity*
In two dimensions, the numerical phase velocity depends not only on the wave-number, but also on the propagation direction. Compared to the true phase speed, any dependency on direction is erroneous. Consequently, the isotropy error of the numerical phase speed should be as low as possible to represent the physical situation well.

(3) *Isotropy of the time step limit*
This requirement has purely numerical reasons. For explicit time integration, the time step limit is a function of the angle of propagation, i.e. the stability limit depends on the local orientation of the differencing stencil with respect to the global coordinate system. As a consequence, an isotropic stability limit is desired to achieve a time step limit, which is independent of the local orientation of the stencil.

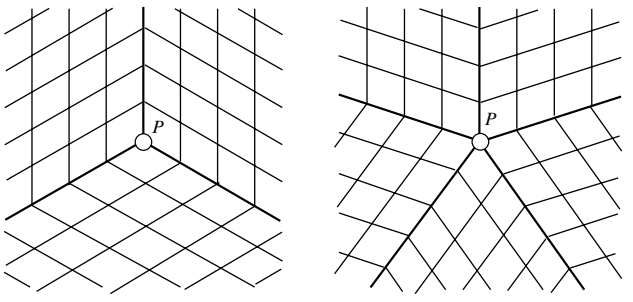

Fig. 1. Examples of grid singularities. Left: three-way singularity; right: five-way singularity.

(4) *Formal order of accuracy*
The finite difference schemes for grid singularities should be compatible in terms of formal order of accuracy with finite differences used in the regular parts of the computational mesh. Therefore, the order of accuracy should be as high as possible.

The requirements on schemes for grid singularities can be summarized as follows:

– non-dissipative schemes of high formal order of accuracy,
– low isotropy error in phase speed, and
– time step limit independent of propagation direction.

4. Three-way singularities

4.1. Differencing stencil

As a consequence of the requirement for non-dissipative schemes, only symmetric differencing stencils are considered. Referring to (8), the arrangement of points in the stencil has to be symmetric with respect to both the x- and the y-axis. For that reason, additional diagonal points are employed so that symmetric 6-, 12-, and 18-point stencils can be constructed, Fig. 2. It has to be noted, that these additional points are located on grid-line intersections. Hence, no interpolation of the depending variable at the additional position is necessary.

4.2. Coefficients for the 6-point scheme

As discussed in the previous section, the finite difference approximation should possess several characteristics. According to these requirements the coefficients are determined.

Formal order of accuracy. Based on two-dimensional Taylor series expansions, the highest achievable order for the 6-point scheme is second. This requirement still leaves two coefficients undetermined: one coefficient for the approximation of the x-derivative, and one for the y-derivative.

Non-dissipative approximation. From the requirement on the real part of the spectral function to vanish, antisymmetric coefficients are demanded for both sets of coefficients a_x and a_y, respectively, e.g.,

$$a_{x,2} = -a_{x,6}. \tag{9}$$

Taken these constraints into account, there still remains one coefficient of the a_y-set undetermined. It is found such that the isotropy of the phase speed of the emerging differencing scheme is optimized, i.e. the isotropy error of the phase velocity is minimized.

The resulting system of equation is solved for the coefficients $a_{x,i}$ and $a_{y,i}$. For the 6-point scheme, the following scheme emerges,

$$\left.\frac{\partial U}{\partial x}\right|_P \approx \frac{1}{L}\sum_{i=1}^{6} a_{x,i}u_i, \quad \text{and} \quad \left.\frac{\partial U}{\partial y}\right|_P \approx \frac{1}{L}\sum_{i=1}^{6} a_{y,i}u_i, \tag{10}$$

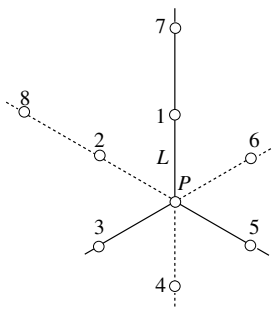

Fig. 2. Part of the node arrangement and numbering system for the 6-, 12-, and 18-point stencil. (Points on dashed lines denote additional positions.)

with

$$a_{x,i} = \left\{0, -\frac{\sqrt{3}}{6}, -\frac{\sqrt{3}}{6}, 0, \frac{\sqrt{3}}{6}, \frac{\sqrt{3}}{6}\right\}, \quad \text{and} \quad a_{y,i} = \left\{\frac{1}{3}, \frac{1}{6}, -\frac{1}{6}, -\frac{1}{3}, -\frac{1}{6}, \frac{1}{6}\right\}. \tag{11}$$

According to (7) the ratio of numerical phase velocity to true phase velocity is given by

$$\frac{c^*}{c} = \frac{2}{3}\frac{1}{kL}\left\{\sqrt{3}\mathrm{c}_\alpha \cos\left(\frac{kL}{2}\mathrm{s}_\alpha\right)\sin\left(\sqrt{3}\frac{kL}{2}\mathrm{c}_\alpha\right) + \mathrm{s}_\alpha\left[\cos\left(\sqrt{3}\frac{kL}{2}\mathrm{c}_\alpha\right)\sin\left(\frac{kL}{2}\mathrm{s}_\alpha\right) + \sin(kL\mathrm{s}_\alpha)\right]\right\}, \tag{12}$$

where the abbreviations s_α and c_α are used for the trigonometric functions $\sin\alpha$ and $\cos\alpha$, respectively. This result is plotted in Fig. 3 for different values of dimensionless wave-length $\lambda/L = 2, 3, 4$, and 8.

The leading term in the isotropy error of the numerical phase velocity is independent of propagation direction,

$$\epsilon = \frac{1}{2}\left(\frac{kL}{2}\right)^2 + \mathrm{HOT}, \tag{13}$$

with HOT denoting higher order terms. The numerical phase velocity is very isotropic for wave-lengths $\lambda/L \geqslant 3$. For smaller wave-lengths, the 60 degree direction exhibits slightly higher values. This 6-point scheme was presented in a very similar form in [7].

4.3. 12-Point scheme and 18-point scheme

The same procedure for the computation of the coefficients as for the 6-point scheme is carried out for the coefficients of the 12-point and the 18-point finite difference schemes. Coefficients are found to yield approximations of highest order, that is fourth order for the 12-point scheme, and sixth order for the 18-point scheme in both directions x and y, respectively. Satisfying the requirements for non-dissipative approximations, one coefficient for the approximation of the y-derivative remains free for both schemes. Again, it is chosen to minimize the dependency of the isotropy error of the numerical phase velocity on propagation angle α. The emerging coefficients are listed in Appendices A and B, respectively. The resulting normalized phase velocity for the 12-point scheme is

$$\frac{c^*}{c} = \frac{4}{3}\frac{c^*_{(6)}}{c} - \frac{1}{9}\frac{1}{kL}\left\{\mathrm{s}_\alpha \sin(2kL\mathrm{s}_\alpha) + \sqrt{3}\mathrm{c}_\alpha \cos(kL\mathrm{s}_\alpha)\sin(\sqrt{3}kL\mathrm{c}_\alpha) + \mathrm{s}_\alpha \sin(kL\mathrm{s}_\alpha)\cos(\sqrt{3}kL\mathrm{c}_\alpha)\right\}, \tag{14}$$

with $c^*_{(6)}$ denoting the numerical phase velocity of the 6-point scheme. The result is plotted in Fig. 4.

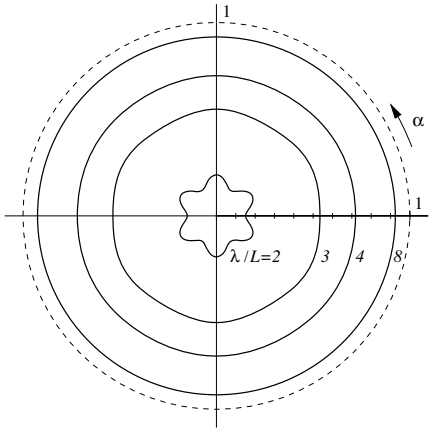

Fig. 3. Polar diagram of the normalized numerical phase velocity c^*/c as a function of dimensionless wave-length λ/L and propagation angle α for the 6-point scheme.

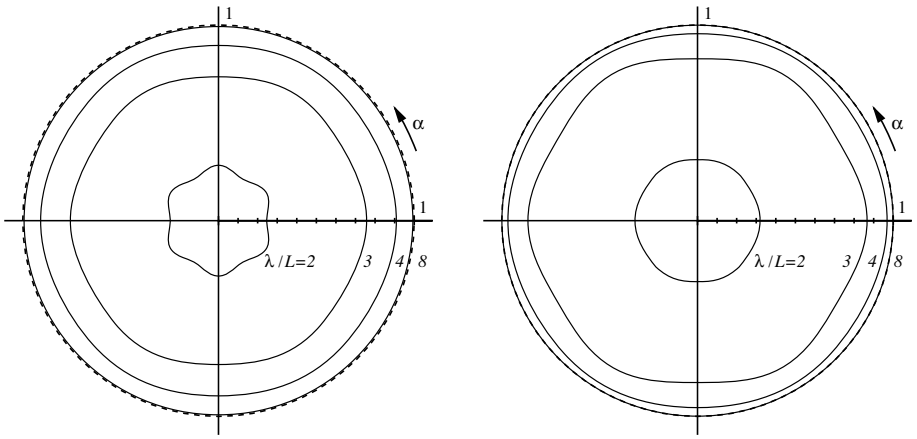

Fig. 4. Polar diagram of the normalized numerical phase velocity c^*/c as a function of dimensionless wave-length λ/L and propagation direction α. Left: 12-point scheme, right: 18-point scheme.

The numerical phase velocity is clearly improved compared to the 6-point scheme, both in dependency on direction and in absolute value. The leading term of the isotropy error of the numerical phase velocity is not independent of α, though its dependency is minimized,

$$\epsilon = \frac{1}{30}\left(\frac{kL}{2}\right)^4 [10 - \cos(6\alpha)] + \text{HOT}. \tag{15}$$

The numerical phase velocity for the 18-point scheme is found to be

$$\frac{c^*}{c} = \frac{9}{10}\left(-\frac{c^*_{(6)}}{c} + 2\frac{c^*_{(12)}}{c}\right) + \frac{1}{90}\frac{1}{kL}\left\{2\mathrm{s}_\alpha \sin(3kL\mathrm{s}_\alpha) + (\sqrt{3}\mathrm{c}_\alpha - \mathrm{s}_\alpha)\sin\left[\frac{3kL}{2}(\sqrt{3}\mathrm{c}_\alpha - \mathrm{s}_\alpha)\right] + (\sqrt{3}\mathrm{c}_\alpha + \mathrm{s}_\alpha)\sin\left[\frac{3kL}{2}(\sqrt{3}\mathrm{c}_\alpha + \mathrm{s}_\alpha)\right]\right\}, \tag{16}$$

with $c^*_{(12)}$ being the numerical phase velocity of the 12-point scheme. It is plotted in Fig. 4. As expected, the numerical phase velocity is again improved compared to the 12-point scheme. For example, the normalized numerical phase velocity c^*/c for $\lambda/L = 8$ is

$$0.999000 < \frac{c^*}{c} < 0.999356,$$

and

$$0.955310 < \frac{c^*}{c} < 0.968447$$

for $\lambda/L = 4$, which are very satisfactory results compared to the exact value of unity. The leading term of the isotropy error of the numerical phase speed is given by

$$\epsilon = \frac{1}{140}\left(\frac{kL}{2}\right)^6 [35 - 8\cos(6\alpha)] + \text{HOT}. \tag{17}$$

5. Five-way singularities

The requirement for non-dissipative approximations demands symmetric differencing stencils also for five-way singularities. Therefore, additional points in diagonal directions are introduced with the same point-to-point distance L. In this way, a symmetric 10-point and 20-point differencing stencil can be constructed, Fig. 5. In contrast to the differencing stencils for three-way singularities, those additional positions are not

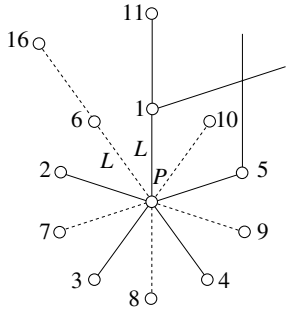

Fig. 5. Part of the node arrangement for five-way singularities. (Points on dashed lines denote additional positions.)

located on grid-line intersections. A coordinate transformation is employed to map the symmetric stencil from the computational domain to the five-way singularity of the physical grid,

$$\frac{\partial U}{\partial x} = \xi_x \frac{\partial U}{\partial \xi} + \eta_x \frac{\partial U}{\partial \eta}, \quad \text{and} \quad \frac{\partial U}{\partial y} = \xi_y \frac{\partial U}{\partial \xi} + \eta_y \frac{\partial U}{\partial \eta}, \tag{18}$$

with

$$\left.\frac{\partial U}{\partial \xi}\right|_i \approx \sum_{j=1}^{N} a_{\xi,j} u_{i+j}, \quad \text{and} \quad \left.\frac{\partial U}{\partial \eta}\right|_i \approx \sum_{j=1}^{N} a_{\eta,j} u_{i+j}, \tag{19}$$

where ξ and η are the coordinates in computational space, and subscripts denote derivation with respect to the corresponding direction x and y, respectively. Metrics in the singular point are found by the Jacobi-matrix using the symmetric 10-point or 20-point scheme to evaluate derivatives.

The coefficients are developed for the symmetric stencil, i.e. in computational space. Subsequently, the coordinate transformation is performed. This procedure avoids any interpolation of the dependent variable at the additional positions. If the points on grid-line intersections were used as additional positions, the resulting differencing stencils were not symmetric, hence violating the requirement for dissipation-free approximations. The property of no dissipation of the scheme is not affected by the coordinate transformation.

For both the 10-point and 20-point scheme, coefficients are found such that the approximations are of highest order in ξ- and η-direction, respectively. Additionally, the coefficients have to fulfill conditions to ensure non-dissipative schemes.

5.1. Symmetric 10-point scheme

The achievable order of the 10-point scheme is second. Conditions for non-dissipative approximations taken into account, there remains one free coefficient for the approximation of the ξ-derivative and two free coefficients for the η-derivative. These free coefficients are found by minimizing the isotropy error of the numerical phase velocity. The following coefficients emerge,

$$\begin{aligned}
a_{\xi,i} = \Bigg\{ & 0, -\frac{1}{10}\sqrt{\frac{1}{2}(5+\sqrt{5})}, -\frac{1}{10}\sqrt{\frac{1}{2}\left(5-\sqrt{5}\right)}, \frac{1}{10}\sqrt{\frac{1}{2}\left(5-\sqrt{5}\right)}, \frac{1}{10}\sqrt{\frac{1}{2}(5+\sqrt{5})}, \\
& -\frac{1}{10}\sqrt{\frac{1}{2}(5-\sqrt{5})}, -\frac{1}{10}\sqrt{\frac{1}{2}\left(5+\sqrt{5}\right)}, 0, \frac{1}{10}\sqrt{\frac{1}{2}\left(5+\sqrt{5}\right)}, \frac{1}{10}\sqrt{\frac{1}{2}(5-\sqrt{5})} \Bigg\}, \\
a_{\eta,i} = \Bigg\{ & \frac{1}{5}, -\frac{1}{20}(1-\sqrt{5}), -\frac{1}{20}(1+\sqrt{5}), -\frac{1}{20}(1+\sqrt{5}), -\frac{1}{20}(1-\sqrt{5}), \\
& \frac{1}{20}(1+\sqrt{5}), \frac{1}{20}(1-\sqrt{5}), -\frac{1}{5}, \frac{1}{20}(1-\sqrt{5}), \frac{1}{20}(1+\sqrt{5}) \Bigg\}.
\end{aligned} \tag{20}$$

The normalized numerical phase velocity of the symmetric scheme is given by

$$\frac{c^*}{c} = \frac{4}{5}\frac{1}{kL}\left\{\frac{1}{2}s_\alpha \sin(kLs_\alpha) + \frac{1+\sqrt{5}}{4}s_\alpha \cos\left[\frac{kL}{2}\sqrt{\frac{1}{2}(5-\sqrt{5})}c_\alpha\right]\sin\left[kL\frac{1+\sqrt{5}}{4}s_\alpha\right]\right.$$
$$+\frac{1-\sqrt{5}}{4}s_\alpha \cos\left[\frac{kL}{2}\sqrt{\frac{1}{2}\left(5+\sqrt{5}\right)}c_\alpha\right]\sin\left[kL\frac{1-\sqrt{5}}{4}s_\alpha\right] + \frac{1}{2}\sqrt{\frac{1}{2}(5-\sqrt{5})}c_\alpha \sin\left[\frac{kL}{2}\sqrt{\frac{1}{2}(5-\sqrt{5})}c_\alpha\right]$$
$$\left.\times \sin\left[kL\frac{1+\sqrt{5}}{4}s_\alpha\right] + \frac{1}{2}\sqrt{\frac{1}{2}(5+\sqrt{5})}c_\alpha \sin\left[\frac{kL}{2}\sqrt{\frac{1}{2}(5+\sqrt{5})}c_\alpha\right]\sin\left[kL\frac{1-\sqrt{5}}{4}s_\alpha\right]\right\}. \quad (21)$$

In Fig. 6 the result is plotted as a function of propagation angle α for different values of the wave-length. Obviously, the isotropy error is very small. It is independent on direction α up to terms of sixth order,

$$\epsilon = \frac{1}{2}\left(\frac{kL}{2}\right)^2 - \frac{1}{12}\left(\frac{kL}{2}\right)^4 + \frac{1}{144}\left(\frac{kL}{2}\right)^6 + \text{HOT}. \quad (22)$$

5.2. Symmetric 20-point scheme

The coefficients for the 20-point differencing scheme are found in a similar way as for the 10-point scheme. The emerging approximations of the ξ- and η-derivatives are of fourth order. Taking conditions for non-dissipative approximations into account, one coefficient for the ξ-derivative and three coefficients for the η-derivative remain undetermined. Again, those coefficients are chosen to reduce the dependency of the phase speed error on propagation angle α to a minimum. The resulting coefficients are listed in Appendix C. The ratio of numerical phase velocity to true phase velocity is found to be

$$\frac{c^*}{c} = \frac{4}{3}\frac{c^*_{(10)}}{c} - \frac{1}{30}\frac{1}{kL}\left\{2s_\alpha \sin(2kLs_\alpha) + (1+\sqrt{5})s_\alpha \cos\left[\frac{kL}{2}\sqrt{2(5-\sqrt{5})}c_\alpha\right]\sin\left[\frac{kL}{2}(1+\sqrt{5})s_\alpha\right]\right.$$
$$+(1-\sqrt{5})s_\alpha \cos\left[\frac{kL}{2}\sqrt{2(5+\sqrt{5})}c_\alpha\right]\sin\left[\frac{kL}{2}(1-\sqrt{5})s_\alpha\right] + \sqrt{2(5-\sqrt{5})}c_\alpha \sin\left[\frac{kL}{2}\sqrt{2(5-\sqrt{5})}c_\alpha\right]$$
$$\left.\times \cos\left[\frac{kL}{2}(1+\sqrt{5})s_\alpha\right] + \sqrt{2(5+\sqrt{5})}c_\alpha \sin\left[\frac{kL}{2}\sqrt{2(5+\sqrt{5})}c_\alpha\right]\cos\left[\frac{kL}{2}(1-\sqrt{5})s_\alpha\right]\right\}, \quad (23)$$

with $c^*_{(10)}$ denoting the numerical phase velocity of the 10-point scheme. Fig. 6 shows the result. The isotropy error is very small for all displayed wave-lengths. The isotropy error of the numerical phase velocity is found to be independent of propagation direction up to sixth order,

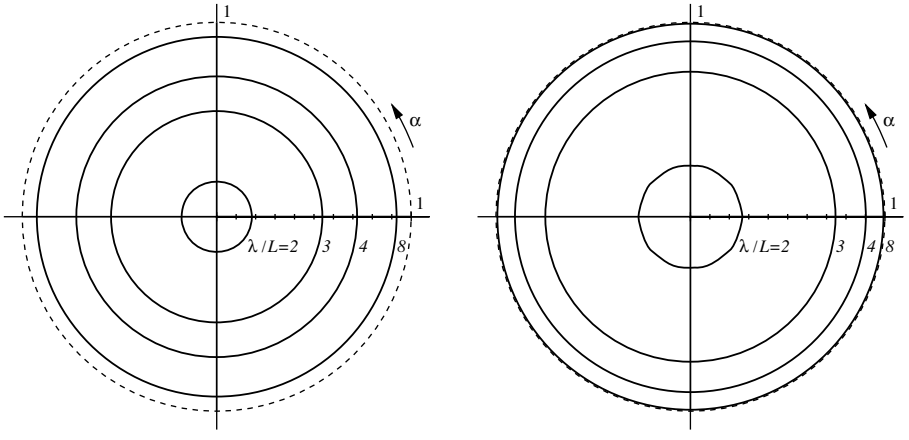

Fig. 6. Polar diagram of the normalized numerical phase velocity c^*/c as a function of dimensionless wave-length λ/L and propagation angle α. Left: symmetric 10-point scheme, right: symmetric 20-point scheme.

$$\epsilon = \frac{1}{3}\left(\frac{kL}{2}\right)^4 - \frac{5}{36}\left(\frac{kL}{2}\right)^6 + \text{HOT}. \tag{24}$$

5.3. Transformation on physical grid

The coefficients $a_{\xi,i}$ and $a_{\eta,i}$ are developed for symmetric schemes, i.e. in computational space. Coordinate transformation maps the symmetric schemes to the physical grid. The metrics is found to be

$$\begin{pmatrix} \xi_x & \eta_x \\ \xi_y & \eta_y \end{pmatrix} = \begin{pmatrix} -3+\sqrt{5}+2\sqrt{5-2\sqrt{5}} & 0 \\ 0 & -3+\sqrt{5}+2\sqrt{5-2\sqrt{5}} \end{pmatrix}. \tag{25}$$

The approximations of the derivatives in Cartesian frame reduce to, e.g. for the x-direction,

$$\frac{\partial U}{\partial x} = \xi_x \frac{\partial U}{\partial \xi} \approx \xi_x \sum_{i=1}^{M} a_{\xi,i} u_i. \tag{26}$$

It is obvious that multiplication by the metric factor does not change the property of no dissipation of the resulting differencing scheme. The coefficients in physical space are, consequently,

$$a_{x,i} = a_{\xi,i}\xi_x, \quad \text{and} \quad a_{y,i} = a_{\eta,i}\eta_y. \tag{27}$$

6. Stability limits

Stability limits of the developed differencing schemes are investigated using the linear two-dimensional convection equation (1). As a representative for explicit numerical time integration the classical four stage Runge–Kutta method of fourth order is employed. Conversion of time-step limits to any other explicit time integration scheme is straightforward. As discussed in Section 3, an isotropic time-step limit is desired. The time-step limit is defined in the von Neumann sense of stability [17]: a numerical algorithm is stable, if the amplification factor G

$$|G(k,\alpha)| \leqslant 1.$$

Time-step limits for the developed difference schemes are presented in Fig. 7 in terms of the Courant-number $(|\vec{c}|\Delta t)/L$. It shows that numerical stability is almost independent of propagation direction. The time-step limits of the presented schemes are similar to or greater than those of regular schemes with the same order of accuracy. In Fig. 8 the stability limits of the current schemes for three-way singularities are compared to limits of central differencing schemes of second, fourth and sixth order. For the case of second order schemes, the

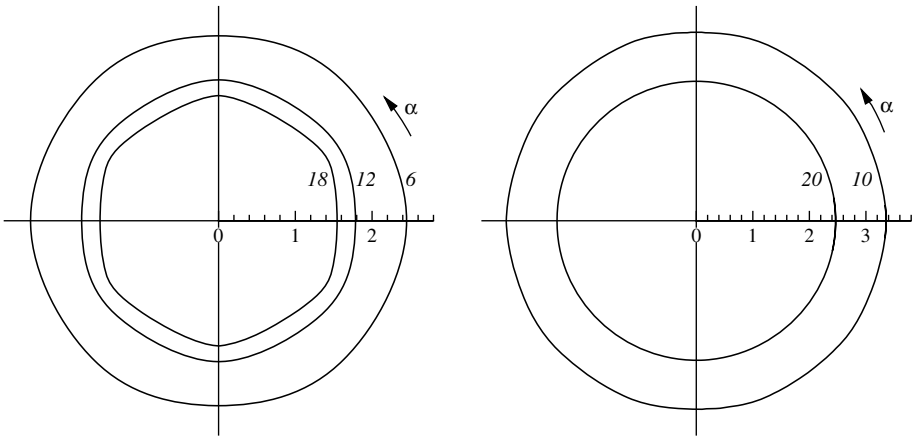

Fig. 7. Time step limits in terms of Courant number for the two-dimensional linear wave-equation and explicit Runge–Kutta integration as a function of α. Left: 6-, 12-, and 18-point scheme; right: 10- and 20-point scheme on physical grid.

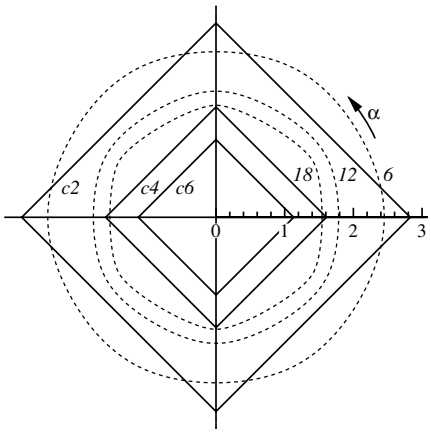

Fig. 8. Comparison of time-step limits of schemes for grid singularities with central differencing schemes. Solid lines: central differencing of second (c2), fourth (c4) and sixth (c6) order; dashed lines: 6-, 12-, and 18-point scheme.

6-point scheme has a higher stability limit in the range $10° < \alpha < 80°$. In the cases of fourth and sixth order schemes, the 12-point and 18-point schemes exhibit a significant greater stability limit than the comparable regular schemes. This indicates that the presented schemes can be combined in a computational mesh with regular schemes of same order of accuracy without limiting the overall time-step of the computation.

The same applies for the five-way schemes. Both exhibit a greater stability limit than corresponding regular differencing schemes.

7. Discussion of results

Finite difference approximations for first derivatives have been developed for three-way and five-way grid singularities. The differencing schemes for three-way singularities are based on symmetric point arrangements with six branches, consequently, they can directly be applied for six-way grid singularities. The schemes for five-way singularities may be applied in their symmetrical form for ten-way grid singularities.

In the previous sections it was shown that the developed schemes are compatible in terms of time step limits with regular schemes of the same order of accuracy. The numerical phase speed should correspond with those of comparable regular schemes as well; they are compared for the three-way schemes in Fig. 9.

The phase speeds of the three-way schemes are well within the range of phase-speeds of compatible regular schemes, which exhibit a greater anisotropy. Hence, the three-way schemes are well suited to be combined with regular schemes of the same order of accuracy.

The five-way schemes exhibit greater errors in numerical phase speed, Fig. 10. This is due to the coordinate transformation, which maps the symmetric schemes to the physical grid. In this context it has to be noted that

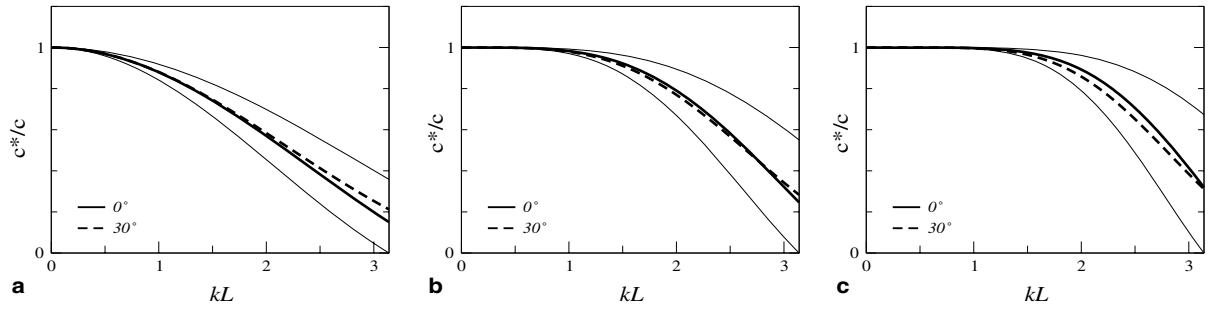

Fig. 9. Ratio of numerical phase velocity to true phase velocity of schemes for three-way singularities: (a) 6-point scheme and central differencing (CD) second order, (b) 12-point scheme and CD fourth order, (c) 18-point scheme and CD sixth order. (Thin lines denote the range of wave-speeds for regular schemes.)

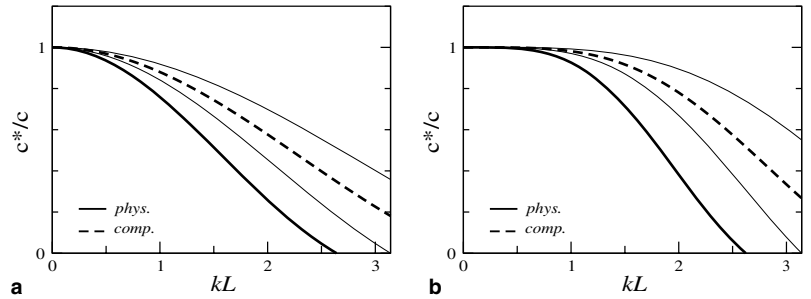

Fig. 10. Ratio of numerical phase velocity to true phase velocity of schemes for five-way singularities: (a) 10-point scheme and central differencing (CD) second order, (b) 20-point scheme and CD fourth order. (Thin lines denote the range of wave-speeds for regular schemes; bold solid line: physical grid, bold dashed line: computational grid.)

the presented difference approximations are intended to be used in geometrically singular points, and not throughout the whole domain of computation. Furthermore, higher stability limits allow smaller point-to-point distances, which compensate the greater error in numerical phase speed. All schemes have been developed based on symmetric stencils. Their use on non-symmetric stencils can be accomplished straightforward using coordinate transformation. It is important to note that the property of no dissipation is not affected by the transformation. Consequently, the schemes remain numerically stable.

8. Numerical experiments

8.1. Formal order of accuracy

The formal order of accuracy of the proposed schemes is verified by solving the two-dimensional convection equation (1) numerically on a finite rectangular domain extending 160 L in x-direction and 120 L in y-direction. For the initial condition a Gaussian distribution is applied,

$$U(x,y,0) = \exp\left[-\ln 2\frac{(x-60)^2+(y-45)^2}{6^2}\right].$$

To avoid any influences of boundary formulations and corresponding discretizations, periodic boundaries are prescribed at the borders of the domain. For the refinement studies, the same geometry and initial condition is used, whereas the point-to-point distances of the computational meshes are halved gradually. All calculations are performed for a time period of 200, using an absolute propagation speed of unity and a propagation direction parallel to the diagonal of the geometry. After that period of time, the initial distribution has traversed the domain once.

Time is integrated by the classical four step Runge–Kutta method of fourth order. The Courant-number is kept constant on a low level for each refinement study, so that the error of time integration will not corrupt the spatial error. Preliminary numerical experiments showed a Courant-number of *0.1* to be sufficiently small. The global error is measured by the L_2-norm of the local errors,

$$L_2 = \sqrt{\sum_i (u_i - U_i)^2},$$

where U is the exact solution at the corresponding discrete position at time 200.

The schemes for three-way singularities are evaluated on regular triangular meshes with an initial point-to-point distance L. Consequently, the coarsest computational mesh consists of 185 points in x-direction, and 120 points in y-direction, respectively. Due to the regular grid the differencing schemes are applied directly to approximate the spatial derivatives.

Fig. 11a shows the global error as the mesh is refined. Obviously, the numerical solution converges to the exact solution with second order for the 6-point scheme, with fourth order for the 12-point scheme, and with sixth order using the 18-point scheme, respectively.

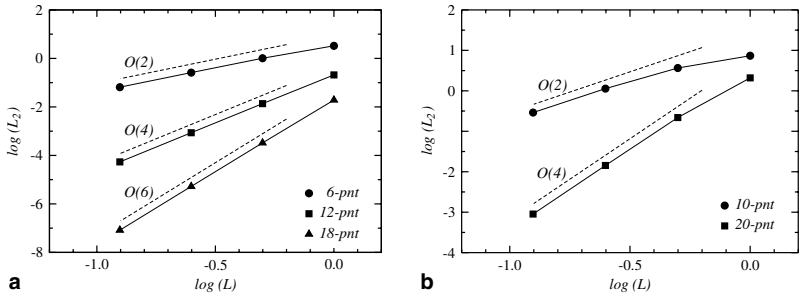

Fig. 11. Reduction of the global error with refined grids: (a) schemes for three-way singularities, (b) schemes for five-way singularities. (Dashed lines denote slopes of 2, 4, and 6 in logarithmic scale.)

Since a mesh for a regular five-point (or ten-point) arrangement can not be constructed in the plane, Cartesian grids are used to evaluate the performance of the differencing schemes for five-way singularities. The geometrical point arrangement is such that the points of the differencing stencils coincide with Cartesian mesh points. Fig. 12 illustrates the node-arrangement for the 10-point scheme, a similar arrangement is used for the 20-point stencil. As a consequence, a coordinate transformation has to be introduced to compensate the distortion of the point-arrangement. The evaluation of the metrics is based on the same differencing scheme as the approximations of derivatives of the dependent variable. As a result, the order of accuracy of the numerical differentiation will be kept at the proposed level. Fig. 11b shows the error norms as a function of the mesh density. The global error tends to zero with second order for the 10-point scheme, and with fourth order for the 20-point scheme.

8.2. Scattering from circular cylinders

As an example for the application of the proposed schemes the scattering of sound by three spatially distributed circular cylinders is chosen. This example has been proposed as a benchmark problem for high-order computational aeroacoustics codes by Visbal [18] to test the ability of a code to handle complex geometries. For this problem, an analytic solution is available, e.g., Sherer [19].

The acoustic scattering problem is governed by the linearized Euler equations, which may be written in dimensionless form for two spatial coordinates as

$$\begin{aligned}
&\frac{\partial \rho}{\partial t}+\frac{\partial u}{\partial x}+\frac{\partial v}{\partial y}=0,\\
&\frac{\partial u}{\partial t}+\frac{\partial p}{\partial x}=0,\\
&\frac{\partial v}{\partial t}+\frac{\partial p}{\partial y}=0,\\
&\frac{\partial p}{\partial t}+\frac{\partial u}{\partial x}+\frac{\partial v}{\partial y}=S.
\end{aligned} \tag{28}$$

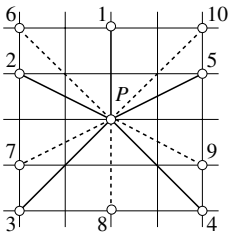

Fig. 12. Positions of nodes on a Cartesian grid for the 10-point scheme.

The flow variables have been non-dimensionalized with the diameter of the larger cylinder $D_{\max}$ as length-scale, ambient speed of sound c_∞ as velocity scale, and $D_{\max}/c_\infty$ as time-scale. Density is non-dimensionalized by the ambient density ρ_∞, and pressure by $\rho_\infty c_\infty^2$. The time dependent acoustic source is

$$S = \exp\left[-\ln 2\frac{(x^2+y^2)}{b^2}\right]\sin(\omega t),$$

with a time frequency $\omega = 8\pi$ and a half-height radius $b = 0.2$. Fig. 13 shows the arrangement of the cylinders and the computational domain, which consists of 94 blocks.

An additional square block has been introduced at the centerline right of the two smaller cylinders to enforce the appearance of three-way singularities. All in all, the computational grid comprises 16 five-way singularities and 4 three-way singularities. The governing equations are solved using spectrally tuned finite difference approximations for the spatial derivatives [14]. Discretization in the singular points is performed using the proposed 12-point scheme for the three-way singularities, and the 20-point scheme for the five-way singularities, respectively, so that all spatial derivatives are approximated by fourth order schemes. Time is integrated by the explicit four step Runge–Kutta method of fourth order. Radiation conditions are applied at the borders of the domain. The surfaces of the three cylinders are considered rigid.

The computational grid consists of 2.33×10^5 points, resulting in a resolution of approximately 8 points per wave-length. The calculation is carried out for a time period of 50 using a time step of 0.005. After that period, the initial transient has left the domain and a periodic state is reached. Fig. 14 shows the distribution of the root-mean-square (RMS) pressure p_{rms} in time-periodic state. For a quantitative comparison, the distribution

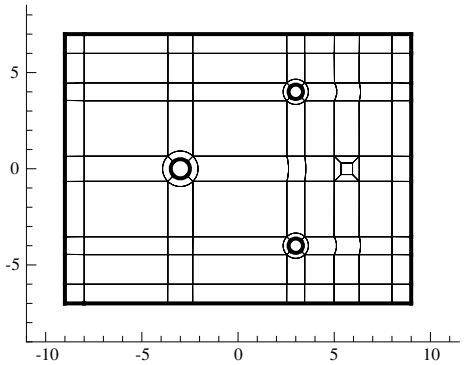

Fig. 13. Calculation domain and arrangement of blocks for scattering problem.

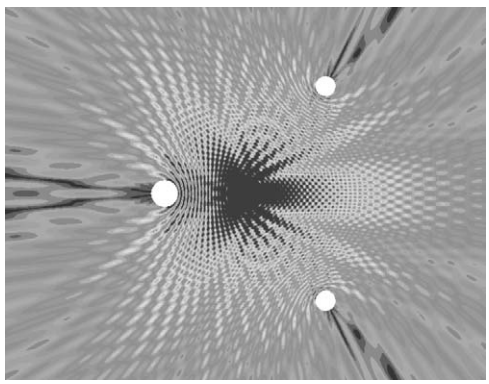

Fig. 14. Root-mean-square pressure contours for scattering problem.

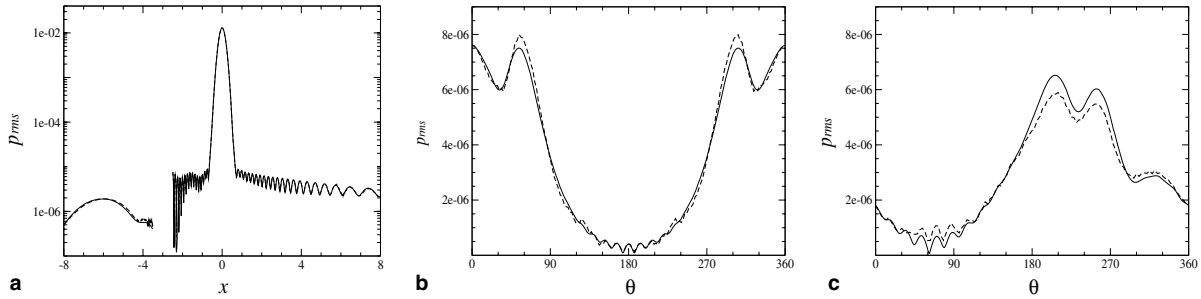

Fig. 15. Comparison of numerically obtained RMS pressure with analytic solution: (a) centerline, (b) surface of left cylinder, (c) surface of upper right cylinder. (Dashed line: numerical, solid line: analytic.)

of p_{rms} along the centerline and along the surfaces of the left and the upper right cylinder are compared to the analytic solution, showing very good agreement, Fig. 15.

9. Summary and conclusion

Finite difference approximations of first derivatives have been developed for two-dimensional three-way and five-way grid singularities. The schemes for three-way singularities are designed such that they can directly be used for six-way singularities.

The developing criteria are to apply the schemes in combination with conventional differencing schemes. For that purpose, they should exhibit similar, or preferably better, characteristics in terms of isotropy of the phase speed, numerical stability and absolute numerical phase velocity than regular finite differences. Free coefficients have been used to formulate constraints to achieve those objectives. Stability limits and spectral characteristics imply that the schemes may favorably be used together with regular four-branch finite-difference schemes of the same formal order of accuracy.

The formal order of accuracy of the schemes has been verified. The application of the proposed schemes to a benchmark problem shows their practical usability.

Acknowledgement

The author would like to express his thanks to the Technical Acoustics Division of the German Aerospace Center for kindly providing the code PIANO.

Appendix A. Coefficients for the 12-point scheme

$$a_{x,i} = \left\{0, -\frac{2\sqrt{3}}{9}, -\frac{2\sqrt{3}}{9}, 0, \frac{2\sqrt{3}}{9}, \frac{2\sqrt{3}}{9}, 0, \frac{\sqrt{3}}{36}, \frac{\sqrt{3}}{36}, 0, -\frac{\sqrt{3}}{36}, -\frac{\sqrt{3}}{36}\right\},$$

$$a_{y,i} = \left\{\frac{4}{9}, \frac{2}{9}, -\frac{2}{9}, -\frac{4}{9}, -\frac{2}{9}, \frac{2}{9}, -\frac{1}{18}, -\frac{1}{36}, \frac{1}{36}, \frac{1}{18}, \frac{1}{36}, -\frac{1}{36}\right\}.$$

Appendix B. Coefficients for the 18-point scheme

$$a_{x,i} = \left\{0, -\frac{\sqrt{3}}{4}, -\frac{\sqrt{3}}{4}, 0, \frac{\sqrt{3}}{4}, \frac{\sqrt{3}}{4}, 0, \frac{\sqrt{3}}{20}, \frac{\sqrt{3}}{20}, 0, -\frac{\sqrt{3}}{20}, -\frac{\sqrt{3}}{20}, 0, -\frac{\sqrt{3}}{180}, -\frac{\sqrt{3}}{180}, 0, \frac{\sqrt{3}}{180}, \frac{\sqrt{3}}{180}\right\},$$

$$a_{y,i} = \left\{\frac{1}{2}, \frac{1}{4}, -\frac{1}{4}, -\frac{1}{2}, -\frac{1}{4}, \frac{1}{4}, -\frac{1}{10}, -\frac{1}{20}, \frac{1}{20}, \frac{1}{10}, \frac{1}{20}, -\frac{1}{20}, \frac{1}{90}, \frac{1}{180}, -\frac{1}{180}, -\frac{1}{90}, -\frac{1}{180}, \frac{1}{180}\right\}.$$

Appendix C. Coefficients for the symmetric 20-point scheme

$$
\begin{aligned}
a_{\xi,i} = \Bigg\{ & 0, \frac{-1}{15}\sqrt{2(5+\sqrt{5})}, \frac{-1}{15}\sqrt{2(5-\sqrt{5})}, \frac{1}{15}\sqrt{2(5-\sqrt{5})}, \frac{1}{15}\sqrt{2(5+\sqrt{5})}, \\
& \frac{-1}{15}\sqrt{2(5-\sqrt{5})}, \frac{-1}{15}\sqrt{2(5+\sqrt{5})}, 0, \frac{1}{15}\sqrt{2(5+\sqrt{5})}, \frac{1}{15}\sqrt{2(5-\sqrt{5})}, \\
& 0, \frac{1}{120}\sqrt{2(5+\sqrt{5})}, \frac{1}{120}\sqrt{2(5-\sqrt{5})}, \frac{-1}{120}\sqrt{2(5-\sqrt{5})}, \frac{-1}{120}\sqrt{2(5+\sqrt{5})}, \\
& \frac{1}{120}\sqrt{2(5-\sqrt{5})}, \frac{1}{120}\sqrt{2(5+\sqrt{5})}, 0, \frac{-1}{120}\sqrt{2(5+\sqrt{5})}, \frac{-1}{120}\sqrt{2(5-\sqrt{5})} \Bigg\}, \\
a_{\eta,i} = \Bigg\{ & \frac{4}{15}, \frac{-1}{15}(1-\sqrt{5}), \frac{-1}{15}(1+\sqrt{5}), \frac{-1}{15}(1+\sqrt{5}), \frac{-1}{15}(1-\sqrt{5}), \\
& \frac{1}{15}(1+\sqrt{5}), \frac{1}{15}(1-\sqrt{5}), \frac{-4}{15}, \frac{1}{15}(1-\sqrt{5}), \frac{1}{15}(1+\sqrt{5}), \\
& \frac{-1}{30}, \frac{1}{120}(1-\sqrt{5}), \frac{1}{120}(1+\sqrt{5}), \frac{1}{120}(1+\sqrt{5}), \frac{1}{120}(1-\sqrt{5}), \\
& \frac{-1}{120}(1+\sqrt{5}), \frac{-1}{120}(1-\sqrt{5}), \frac{1}{30}, \frac{-1}{120}(1-\sqrt{5}), \frac{-1}{120}(1+\sqrt{5}) \Bigg\}.
\end{aligned}
$$

References

[1] S.K. Lele, Compact finite difference schemes with spectral-like resolution, J. Comp. Phys. 103 (1) (1992) 16–42.
[2] R.W. Dyson, J.W. Goodrich, Automated approach to very high-order aeroacoustic computations, AIAA J. 39 (3) (2001) 396–406.
[3] R. Hixon, M. Nallasamy, S. Sawyer. Effect of grid singularities on the solution accuracy of a CAA code. AIAA paper 2003-879, 2003.
[4] P.J. Morris, L.N. Long, A. Bangalore, Q. Wang, A parallel three-dimensional computational aeroacoustics method using nonlinear disturbance equations, J. Comp. Phys. 133 (1997) 56–74.
[5] K.C. Chung, A generalized finite-difference method for heat transfer problems of irregular geometries, Numer. Heat Transfer 4 (1981) 345–357.
[6] L. Collatz, The Numerical Treatment of Differential Equations, third ed., Springer, 1960.
[7] D.W. Zingg, H. Lomax, Finite-difference schemes on regular triangular grids, J. Comp. Phys. 108 (1993) 306–313.
[8] R. Mullen, T. Belytschko, Dispersion analysis of finite element semidiscretizations of the two-dimensional wave equation, Int. J. Num. Meth. Eng. 18 (1982) 11–29.
[9] R. Vichnevetsky, J.B. Bowles, Fourier analysis of numerical approximations of hyperbolic equations, SIAM Studies in Applied Mathematics (1982).
[10] R. Vichnevetsky, Wave propagation analysis of difference schemes for hyperbolic equations: a review, Int. J. Numer. Method. Fluids 7 (1987) 409–452.
[11] L.N. Trefethen, Group velocity in finite difference schemes, SIAM Rev. 24 (2) (1982) 113–136.
[12] A. Bamberger, J.C. Guillot, P. Joly, Numerical diffraction by a uniform grid, SIAM J. Numer. Anal. 25 (4) (1988) 753–783.
[13] R. Vichnevetsky, F. De Schutter, A frequency analysis of finite differences and finite-element methods for initial value problems, in: Advances in Computer Methods for Partial Differential Equations. AICA-1975, Rutgers University, NJ, 1975.
[14] C.K.W. Tam, J.C. Webb, Dispersion-relation-preserving finite difference schemes for computational acoustics, J. Comp. Phys. 107 (1993) 262–281.
[15] Z. Haras, S. Ta'asan, Finite difference schemes for long-time integration, J. Comp. Phys. 114 (1994) 265–279.
[16] D.P. Lockard, K.S. Brentner, H.L. Atkins. High accuracy algorithms for computational aeroacoustics. AIAA paper 94-0460, 1994.
[17] R.D. Richtmyer, K.W. Morton, Difference Methods for Initial-Value Problems, second ed., John Wiley & Sons, 1967.
[18] M. Visbal, Benchmark problems category 2 – complex geometry, in: Fourth Computational Aeroacoustics (CAA) Workshop on Benchmark Problems, NASA/CP-2004-212954, NASA Glenn Research Center, 2004, pp. 10–12.
[19] S.E. Sherer, Acoustic scattering from multiple circular cylinders: category 2, problems 1 and 2, analytic solution, in: Fourth Computational Aeroacoustics (CAA) Workshop on Benchmark Problems, NASA/CP–2004-212954, NASA Glenn Research Center, 2004, pp. 39–43.